

Cosmological Parameter Estimation for Dynamical Dark Energy Models with Future Fast Radio Burst Observations

ZE-WEI ZHAO,¹ ZHENG-XIANG LI,² JING-ZHAO QI,¹ HE GAO,² JING-FEI ZHANG,¹ AND XIN ZHANG¹

¹*Department of Physics, College of Sciences, Northeastern University, Shenyang 110819, China; zhangxin@mail.neu.edu.cn*

²*Department of Astronomy, Beijing Normal University, Beijing 100875, China; zxli918@bnu.edu.cn, gaoh@bnu.edu.cn*

ABSTRACT

Fast radio bursts (FRBs) are a mysterious astrophysical phenomenon of bright pulses emitted at radio frequencies, and it is expected for them to be frequently detected in the future. The dispersion measures of FRBs are related to cosmological parameters, and thus FRBs have a potential to be developed into a new cosmological probe if their data can be largely accumulated in the future. In this work, we study the capability of future FRB data for improving cosmological parameter estimation in two dynamical dark energy models. We find that the simulated FRB data can break the parameter degeneracies inherent in the current cosmic microwave background (CMB) data. Therefore, the combination of the CMB and FRB data can significantly improve the constraints on the Hubble constant and dark energy parameters, compared to those using CMB or FRB alone. If ten thousand events of FRBs with known redshifts are detected in the future, they would behave better than the baryon acoustic oscillation (BAO) data in breaking the parameter degeneracies inherent in the CMB data. We also find that the combination of FRB and gravitational wave (GW) standard siren data provides an independent low-redshift probe to verify the results from CMB and BAO data. For the data combination of CMB, GW, and FRB, it is found that the main contribution to the constraints comes from the CMB and GW data, but the inclusion of FRB data still can evidently improve the constraint on the baryon density.

Keywords: fast radio burst, cosmological parameter estimation, dark energy, gravitational wave standard sirens, cosmological probe

1. INTRODUCTION

The late-time cosmic accelerated expansion discovered by Supernova Search Team et al. (1998) and Supernova Cosmology Project et al. (1999) is hardly to be realized in a universe governed by general relativity with only barotropic and pressureless fluids. To realize the acceleration in the late universe, one needs to modify general relativity at the cosmological scale or introduce a new component with negative pressure, called dark energy (DE). The CMB anisotropies data observed by the Planck satellite (Planck Collaboration et al. 2018a) favor the Λ cold dark matter (Λ CDM) model with the DE provided by a cosmological constant (Λ), which is usually regarded as the standard model of cosmology (Bahcall et al. 1999). However, the Λ CDM model suffers from the cosmological constant problem (Weinberg 1989), so the proposal of dynamical dark energy has also been widely studied (Joyce et al. 2015).

The CMB data alone can only measure the parameters at high precision for the base Λ CDM model, but they cannot provide precise measurements for the extra parameters if the model is extended to include new

physics; in particular, there usually exist strong degeneracies between these parameters (Planck Collaboration et al. 2018b). Since the CMB observation is the measurement of the early universe, low-redshift observations like the baryon acoustic oscillation (BAO) observation are employed as complements to break the parameter degeneracies (Beutler et al. 2011; Ross et al. 2015; BOSS Collaboration et al. 2017). It should be pointed out that, although the current BAO measurements come from the galaxy redshift surveys for late universe, the BAO and CMB observations actually share the same standard ruler of the comoving scale of sound horizon formed in the early universe. Thus, developing more independent and precise low-redshift cosmological probes to verify the results from CMB+BAO is of great interest and importance.

Recently, a class of bright pulses with millisecond-duration at radio frequencies, named fast radio bursts (FRBs), has been detected (Lorimer et al. 2007; Thornton et al. 2013; Petroff et al. 2015, 2016). Although the FRBs' specific progenitors are still unknown, their locations are considered to be extragalactic, for the dis-

persion measures (DMs) of them greatly exceeding the maximum Galactic expectations. Indeed, the cosmological redshifts and the host galaxies of several FRBs have been recently identified (Scholz et al. 2016; Spitler et al. 2016; Chatterjee et al. 2017; Marcote et al. 2017; Tendulkar et al. 2017; Bannister et al. 2019; Ravi et al. 2019), including both repeating and non-repeating events. It has long been proposed that a sufficiently large sample of FRBs with redshift detection could be used to place constraints on cosmological parameters through the DM-redshift relation (Gao et al. 2014; Zhou et al. 2014). Current FRB observations suggest a sufficiently high all-sky FRB rate of $\sim 10^3 - 10^4$ per day (Cordes & Chatterjee 2019; Petroff et al. 2019). Started or upcoming surveys, such as the Canadian Hydrogen Intensity Mapping Experiment (CHIME) telescope and its FRB search backend (CHIME/FRB Collaboration et al. 2018), and especially the Square Kilometre Array (SKA) project (Macquart et al. 2015) are expected to detect about one thousand or more FRB events everyday (Fialkov & Loeb 2017), enabling it feasible to constrain cosmological parameters.

In the literature, the cosmological parameter estimation from FRB was pioneered by using the possible association of FRBs and Gamma-Ray Bursts (Deng & Zhang 2014; Gao et al. 2014) and developed into a promising tool to study the expansion history of the universe by a series of works, e.g. breaking the cosmological parameter degeneracies by combining the FRB data with the BAO data (Zhou et al. 2014) and the type Ia supernova (SN) data (Jaroszynski 2019), directly constraining cosmological parameters by introducing a slope parameter (Yang & Zhang 2016), extracting cosmological distance information considering the effects of systematic uncertainties (Kumar & Linder 2019), acting as a cosmological probe from strongly lensed repeating FRBs (Li et al. 2018; Liu et al. 2019), measuring the cosmic proper distance (Yu & Wang et al. 2017), and improving the constraints on baryon density compared to the current data set (Walters et al. 2018). However, the combination of FRB and the current most precise cosmological probe, the CMB observation, is still not deeply studied.

Besides, an interesting and heuristic idea is the gravitational wave (GW)/FRB association proposed by Wei et al. (2018), in which the authors noticed that the combination of luminosity distance d_L from GW and DM of FRB would be very helpful in cosmological tests. Inspired by this idea, Cai et al. (2019) probed cosmic anisotropy with GW/FRB association and Li et al. (2019) introduced a cosmology-independent estimate of the fraction of baryon mass in the intergalactic medium (IGM). It is suggested that the correlations of cosmo-

logical parameters in DM and in d_L are rather different, even opposite, because DM is proportional to the Hubble constant H_0 whereas d_L is inversely proportional to H_0 . This fact may also be very helpful in cosmological parameter estimation and needed to be further studied.

The GWs detected by the Laser Interferometer Gravitational-Wave Observatory (LIGO) are astronomical low-redshift events produced by the mergers of binary black hole or binary neutron-star (BNS) systems, which are fully independent of the high-redshift CMB observation. The advantage of GW is that the absolute distance information of the source can be directly extracted from the GW signal, which discards the distance ladder method to calibrate between different astronomical processes. The GW events observed by the next-generation ground-based GW detectors, such as the Einstein Telescope (ET), combined with independent electromagnetic observations, can lead to a true distance-redshift relation, which can be used to study cosmology. Thus, such GW sources are often dubbed “standard sirens” (Schutz 1986; Holz & Hughes 2005), and are expected to become a new precise cosmological probe (Sathyaprakash et al. 2009; Feeney et al. 2019; Chen et al. 2018; Zhang 2019; Zhang et al. 2019; Wang et al. 2018; Cai & Yang 2017; Cai et al. 2018; Sathyaprakash et al. 2010; Zhao et al. 2011; Zhang et al. 2020, 2019; Jin et al. 2020; Li 2015; Li et al. 2019). In particular, it is found that the combination of GW and other cosmological probes, such as CMB and BAO, is greatly helpful in breaking the parameter degeneracies (Wang et al. 2018; Zhang et al. 2019, 2020, 2019; Jin et al. 2020; Zhang 2019).

In this paper, we wish to study the capability of future FRB data to break the cosmological parameter degeneracies inherent in the CMB data from Planck and the GW data from ET.

This paper is organized as follows. In Sec. 2, we briefly introduce the methods for simulating the FRB data and the standard siren data. We show the constraint results and make relevant discussions in Sec. 3. Finally, conclusion is given in Sec. 4.

2. METHODS AND DATA

2.1. Simulation of FRBs

In this work, we study two dynamical dark energy models: the w CDM model with the equation of state (EoS) of DE, $w(z) = p_{\text{de}}(z)/\rho_{\text{de}}(z) = w$, and the Chevallier–Polarski–Linder (CPL) model with the EoS of DE, $w(z) = w_0 + w_a z/(1+z)$ (Chevallier & Polarski 2001; Linder 2003). According to the Friedmann equation, the dimensionless Hubble parameter in the flat uni-

verse is given by

$$E^2(z) = \frac{H^2(z)}{H_0^2} = (1 - \Omega_m) \exp \left[3 \int_0^z \frac{1 + w(z')}{1 + z'} dz' \right] + \Omega_m (1 + z)^3, \quad (1)$$

where $H(z)$ is the Hubble parameter, $H_0 = 100h \text{ km s}^{-1} \text{ Mpc}^{-1}$ is the Hubble constant, and Ω_m is the matter density parameter at present.

In order to generate a mock sample of future detectable FRBs, we first need to assume the redshift distribution of FRBs. Until now, the progenitors of FRBs are not generally identified, so there is no real redshift distribution for FRBs. Therefore, following Li et al. (2019), we phenomenologically assume that the sources of FRBs distribute uniformly (i.e., with constant number density in comoving volume),

$$N_{\text{const}}(z) = \mathcal{N}_{\text{const}} \frac{\tilde{\chi}^2(z)}{H(z)(1+z)} e^{-d_L^2(z)/[2d_L^2(z_{\text{cut}})]}, \quad (2)$$

where $\mathcal{N}_{\text{const}}$ is a normalization factor and $\tilde{\chi}(z)$ is the comoving distance at redshift z . We also include a Gaussian cutoff at redshift $z_{\text{cut}} = 1$ to represent the decrease of the detected FRBs beyond it due to the instrumental signal-to-noise threshold effect.

The observed DM of an FRB is the difference between the highest and lowest frequencies of the pulse, whose contributions are mainly from the FRB's host galaxy, IGM, and the Milky Way (Thornton et al. 2013; Deng & Zhang 2014), i.e.,

$$\text{DM}_{\text{obs}} = \text{DM}_{\text{host}} + \text{DM}_{\text{IGM}} + \text{DM}_{\text{MW}}. \quad (3)$$

Among these components, DM_{IGM} is related to cosmology, which is the integral of the electron number density along the path of FRB-photon traveling. The average value of DM_{IGM} can be expressed by cosmological parameters as

$$\langle \text{DM}_{\text{IGM}} \rangle = \frac{3cH_0\Omega_b f_{\text{IGM}}}{8\pi G m_p} \int_0^z \frac{\chi(z')(1+z') dz'}{E(z')}, \quad (4)$$

where

$$\chi(z) = Y_{\text{H}} \chi_{\text{e,H}}(z) + \frac{1}{2} Y_{\text{He}} \chi_{\text{e,He}}(z). \quad (5)$$

In this expression, Ω_b is the baryon density parameter at present, $f_{\text{IGM}} \simeq 0.83$ is the fraction of baryon mass in the IGM (Shull et al. 2012), m_p is the mass of proton, $Y_{\text{H}} = 3/4$ and $Y_{\text{He}} = 1/4$ are the mass fractions of hydrogen and helium, respectively, and $\chi_{\text{e,H}}$ and $\chi_{\text{e,He}}$ are the ionization fractions for hydrogen and helium, respectively. Since both hydrogen and helium are fully

ionized at $z < 3$, we take $\chi_{\text{e,H}} = \chi_{\text{e,He}} = 1$ (Fan et al. 2006).

From Eq. (3), DM_{IGM} can be measured for an FRB if DM_{obs} , DM_{host} , and DM_{MW} could be determined. Thus the total uncertainty of DM_{IGM} is

$$\sigma_{\text{DM}_{\text{IGM}}} = \left[\sigma_{\text{obs}}^2 + \sigma_{\text{MW}}^2 + \sigma_{\text{IGM}}^2 + \left(\frac{\sigma_{\text{host}}}{1+z} \right)^2 \right]^{1/2}. \quad (6)$$

The observational uncertainty $\sigma_{\text{obs}} = 1.5 \text{ pc cm}^{-3}$ is adopted from the average value of the released data (Petroff et al. 2016). According to the Australia Telescope National Facility pulsar catalogue (Manchester et al. 2005)¹, the average uncertainty of the DM_{MW} for the sources at high Galactic latitude is about 10 pc cm^{-3} . The uncertainty σ_{IGM} describes the deviation of individual event from the mean DM_{IGM} , due to the inhomogeneity of the baryon matter in the IGM. Here we use the fitting form of the results in Li et al. (2019), Faucher-Giguère et al. (2011), and McQuinn (2014). It is difficult to estimate σ_{host} , because it generally depends on the individual properties of an FRB, such as the type of the host galaxy, the location of FRB in the host galaxy, and the near-source plasma. We take $\sigma_{\text{host}} = 30 \text{ pc cm}^{-3}$ as the uncertainty of DM_{host} .

Based on the FRB event rate estimated from the current detections, future mid-frequency component of SKA is likely to detect $\sim 10^3 \text{ sky}^{-1} \text{ day}^{-1}$ of FRBs (Fialkov & Loeb 2017). Further assuming that 5% of the detected FRBs can be well-localized to confirm their host galaxies and considering the bright emission lines of the host galaxy for the repeating FRB 121102 (Tendulkar et al. 2017), we assume ~ 10 redshifts of FRB host galaxies per night can be detected by optical telescopes (Walters et al. 2018). Thus we consider a normal expectable scenario with the event number of FRBs $N_{\text{FRB}} = 1000$ and an optimistic scenario with $N_{\text{FRB}} = 10000$ for a few years.

2.2. Simulation of Standard Sirens

To simulate the standard siren data from ET, what we need first is also to assume the redshift distribution of GWs (Cai & Yang 2017; Zhao et al. 2011),

$$P(z) \propto \frac{4\pi \tilde{\chi}^2(z) R(z)}{H(z)(1+z)}, \quad (7)$$

where $R(z)$ is the time evolution of the burst rate with the form (Schneider et al. 2001; Cutler & Holz 2009; Cai

¹ <http://www.atnf.csiro.au/research/pulsar/psrcat/>

& Yang 2017)

$$R(z) = \begin{cases} 1 + 2z, & z \leq 1, \\ \frac{3}{4}(5 - z), & 1 < z < 5, \\ 0, & z \geq 5. \end{cases} \quad (8)$$

The GW signal $h(t)$ in general relativity consists of two polarizations and can be formulated with the antenna pattern functions F as

$$h(t) = F_+(\theta, \phi, \psi)h_+(t) + F_\times(\theta, \phi, \psi)h_\times(t), \quad (9)$$

where ψ is the polarization angle and (θ, ϕ) are the location angles of the source in the detector frame. The antenna pattern functions of one Michelson-type interferometer of ET are (Zhao et al. 2011)

$$\begin{aligned} F_+^{(1)}(\theta, \phi, \psi) &= \frac{\sqrt{3}}{2} \left[\frac{1}{2}(1 + \cos^2\theta) \cos(2\phi) \cos(2\psi) \right. \\ &\quad \left. - \cos\theta \sin(2\phi) \sin(2\psi) \right], \\ F_\times^{(1)}(\theta, \phi, \psi) &= \frac{\sqrt{3}}{2} \left[\frac{1}{2}(1 + \cos^2\theta) \cos(2\phi) \sin(2\psi) \right. \\ &\quad \left. + \cos\theta \sin(2\phi) \cos(2\psi) \right]. \end{aligned} \quad (10)$$

Three interferometers of ET have an azimuthal difference of 60° with each other, so the other two antenna pattern functions are $F_{+, \times}^{(2)}(\theta, \phi, \psi) = F_{+, \times}^{(1)}(\theta, \phi + 2\pi/3, \psi)$ and $F_{+, \times}^{(3)}(\theta, \phi, \psi) = F_{+, \times}^{(1)}(\theta, \phi + 4\pi/3, \psi)$.

It is convenient to analyze GW data in the Fourier space. The Fourier transform for a GW signal can be obtained by using the stationary phase approximation,

$$\mathcal{H}(f) = \mathcal{A}f^{-7/6}e^{i\Psi}, \quad (11)$$

where \mathcal{A} is the amplitude in the Fourier space,

$$\begin{aligned} \mathcal{A} &= \frac{1}{d_L} \sqrt{F_+^2(1 + \cos^2\iota)^2 + 4F_\times^2 \cos^2\iota} \\ &\quad \times \sqrt{5\pi/96\pi^{-7/6}\mathcal{M}_c^{5/6}}. \end{aligned} \quad (12)$$

Here, the luminosity distance is given by

$$d_L(z) = \frac{1+z}{H_0} \int_0^z \frac{cdz'}{E(z')}, \quad (13)$$

$\mathcal{M}_c = (1+z)M\eta^{3/5}$ is the observed *chirp mass*, $M = m_1 + m_2$ is the total mass of coalescing binary, m_1 and m_2 are the masses of black hole (BH) or neutron star (NS), and $\eta = m_1m_2/M^2$ is the symmetric mass ratio. The definition of the function Ψ can refer to Sathyaprakash et al. (2009) and Zhao et al. (2011). The parameter ι denotes the inclination angle between the direction of binary's orbital angular momentum and

the line of sight. Experimentally, the short gamma ray bursts (SGRBs) coupled with GWs are supposed to be strongly beamed, which implies that the observations of SGRBs should be orientated nearly face on (i.e., $\iota \simeq 0$). Computationally, when we apply Fisher matrix to the GW waveform, averaging over ι and ψ with the maximal inclination $\iota = 20^\circ$ is roughly equal to taking $\iota = 0$ (Li 2015). Thus, we take $\iota = 0$ and the dependence for ψ drops out in the simulation of mock sample.

Whether a signal is confirmed as the GW detection is determined by the signal-to-noise ratio (SNR) measured by the detector. The combined SNR for the network of ET is

$$\rho = \sqrt{\sum_{i=1}^3 (\rho^{(i)})^2}, \quad (14)$$

where $\rho^{(i)} = \sqrt{\langle \mathcal{H}^{(i)}, \mathcal{H}^{(i)} \rangle}$ is the SNR of the i th interferometer, with the inner product being defined as

$$\langle a, b \rangle = 4 \int_{f_{\text{lower}}}^{f_{\text{upper}}} \frac{\tilde{a}(f)\tilde{b}^*(f) + \tilde{a}^*(f)\tilde{b}(f)}{2} \frac{df}{S_n(f)}, \quad (15)$$

where “ \sim ” denotes the Fourier transform of the function and $S_n(f)$ is the one-side noise power spectral density. For simplicity, we limit the integral interval within $[1 \text{ Hz}, 2f_{\text{LSO}}]$ with $f_{\text{LSO}} = 1/[6^{3/2}2\pi(1+z)M]$, and take the fitting form $S_n(f)$ of ET from Zhao et al. (2011).

As a preliminary forecast, we use the Fisher information matrix method to estimate the instrumental error on the measurement of d_L as

$$\sigma_{d_L}^{\text{inst}} \simeq \sqrt{\left\langle \frac{\partial \mathcal{H}}{\partial d_L}, \frac{\partial \mathcal{H}}{\partial d_L} \right\rangle^{-1}}. \quad (16)$$

With the GW waveform in Eq. (11) and assuming that d_L is independent of other parameters, it is directly to show $\sigma_{d_L}^{\text{inst}} \propto d_L/\rho$. As mentioned above, the inclination angle is set to be 0 in the simulation. However, when we estimate the practical instrumental error of d_L , the influence of ι should be taken into account, because there is a strong degeneracy between ι and d_L . We consider the maximal effect of ι would bring a factor of 2 (between the source being face-on, $\iota = 0$, and edge-on, $\iota = \pi/2$) to the instrumental error for a conservative consideration (Li 2015),

$$\sigma_{d_L}^{\text{inst}} \simeq \frac{2d_L}{\rho}. \quad (17)$$

There is also weak-lensing error caused by the gravity effect of galaxies, which can be approximated as $\sigma_{d_L}^{\text{lens}} =$

$0.05z d_L$. Thus the total error of d_L is

$$\begin{aligned}\sigma_{d_L} &= \sqrt{(\sigma_{d_L}^{\text{inst}})^2 + (\sigma_{d_L}^{\text{lens}})^2} \\ &= \sqrt{\left(\frac{2d_L}{\rho}\right)^2 + (0.05z d_L)^2}.\end{aligned}\quad (18)$$

Based on the estimate in [Sathyaprakash et al. \(2010\)](#) and [Cai & Yang \(2017\)](#), we simulate 1000 standard siren events detected by ET during 10-year lifetime and take the ratio of BHNS (i.e. the binary system of a black hole and a neutron star) and BNS events to be 0.03. We also set the mass distributions in the interval $[1,2] M_\odot$ for NS and $[3,10] M_\odot$ for BH, where M_\odot denotes the solar mass.

Although the instrumental error of d_L is estimated by applying the Fisher matrix method, we use the Markov-chain Monte Carlo analysis ([Lewis & Bridle 2002](#)) to reveal the distinction between different observations. For the current data, we use the ‘‘Planck distance priors’’ derived from the Planck 2018 data release ([Chen et al. 2019](#)), and the BAO measurements from 6dFGS at $z_{\text{eff}} = 0.106$ ([Beutler et al. 2011](#)), SDSS-MGS at $z_{\text{eff}} = 0.15$ ([Ross et al. 2015](#)), and BOSS-DR12 at $z_{\text{eff}} = 0.38, 0.51, \text{ and } 0.61$ ([BOSS Collaboration et al. 2017](#)). In this work, the fiducial values of cosmological parameters are taken to be the best-fit values of CMB+BAO+SN from [Zhang et al. \(2019\)](#).

3. RESULTS AND DISCUSSION

3.1. CMB+FRB

In this subsection, the simulated FRB data are combined with the CMB data to study the help of FRB in cosmological parameter estimation. In [Table 1](#), we list the best-fit value and the standard 1σ error for every cosmological parameter ξ in the w CDM and CPL models. In the following, *FRB1* and *FRB2* denote the FRB data in the normal expectable scenario (i.e., $N_{\text{FRB}} = 1000$) and the FRB data in the optimistic scenario (i.e., $N_{\text{FRB}} = 10000$), respectively.

The constraints from the CMB data are tighter than those from the FRB data in the normal expectable scenario but weaker than those from the FRB data in the optimistic scenario. We find that the constraints on cosmological parameters are evidently improved for both CMB+FRB1 and CMB+FRB2 combinations. To obtain some insights into how this can be achieved, we plot the two-dimensional marginalized posterior probability distribution contours in the Ω_m - w plane for the w CDM model in [Figure 1\(a\)](#). The orientations of the parameter degeneracies formed by CMB and by FRB are rather different, and thus the parameter degeneracies are broken by combining the CMB and FRB data.

It is clearer to see this effect in [Figure 2\(a\)](#) for the FRB data in the optimistic scenario, in which the FRB data provide a tighter constraint on Ω_m compared to CMB. Quantitatively, the current CMB data combined with the simulated FRB1 and FRB2 data can give the relative errors $\varepsilon(w) = 9.7\%$ and $\varepsilon(w) = 4.3\%$, indicating that the constraints are improved by about 59% and 82% compared with those using the CMB data alone, respectively.

In [Figure 1\(b\)](#), we show the marginalized posterior probability distribution contours in the H_0 - $\Omega_b h^2$ plane for the w CDM model. It is obvious that H_0 and $\Omega_b h^2$ cannot be effectively constrained by FRB alone, since DM_{IGM} is proportional to $H_0 \Omega_b$ [see [Eq. \(4\)](#)]. Considering that CMB can constrain $\Omega_b h^2$ at high precision, the inclusion of CMB can break the degeneracy between H_0 and $\Omega_b h^2$ inherent in FRB, resulting in a precise measurement on H_0 . Concretely, the simulated FRB1 data combined with the current CMB data can achieve the relative error $\varepsilon(h) = 4.4\%$, indicating a 56% improvement compared to $\varepsilon(h) = 10\%$ by using the CMB data alone. The effect of the event number of FRB is distinct for the data combination CMB+FRB, as can be seen from [Figure 2\(b\)](#) in which the degeneracy between H_0 and $\Omega_b h^2$ is extremely strong for the FRB data in the optimistic scenario. Increasing the event number of FRB from 1000 to 10000 improves the constraints to $\varepsilon(h) = 1.8\%$, which corresponds to a 82% reduction in the size of the 1σ error of the CMB data.

In the last part of this subsection, we compare the capabilities of the BAO and FRB data on breaking the parameter degeneracies inherent in the CMB data (see the fourth, sixth, and eighth columns of [Table 1](#)). From [Figure 3](#) we find that the constraints from CMB+BAO are tighter than those from CMB+FRB1 but weaker than those from CMB+FRB2 in both the w CDM and CPL models. For example, the 1σ errors on w_0 and w_a are 0.29 and 0.81, respectively, by CMB+BAO, and 0.24 and 0.58, respectively, by CMB+FRB2. Other than that, the BAO data can provide little help on $\Omega_b h^2$ constraint compared with CMB alone. However, compared with the result from CMB, the inclusion of the FRB2 data improves the constraint on $\Omega_b h^2$ by 42% in the w CDM model.

3.2. GW+FRB

In this subsection, we study whether the combination of the simulated FRB and GW data is able to efficiently break the parameter degeneracies. The constraint results are given in [Table 2](#).

From [Figure 4](#), only in the optimistic scenario, the data combination GW+FRB evidently improves the

Table 1. The constraint results of the cosmological parameters in the w CDM and CPL models.

| Model | Parameter | CMB | CMB+BAO | FRB1 | CMB+FRB1 | FRB2 | CMB+FRB2 |
|---------|---------------------|---------------------------|----------------------------|---------------------------|---------------------------|---------------------------|---------------------------|
| w CDM | Ω_m | $0.324^{+0.055}_{-0.074}$ | 0.316 ± 0.013 | $0.285^{+0.072}_{-0.047}$ | $0.310^{+0.024}_{-0.030}$ | $0.307^{+0.018}_{-0.014}$ | 0.312 ± 0.012 |
| | h | $0.676^{+0.061}_{-0.077}$ | $0.674^{+0.013}_{-0.015}$ | > 0.613 | 0.683 ± 0.030 | > 0.614 | 0.680 ± 0.012 |
| | w | $-1.00^{+0.25}_{-0.22}$ | $-0.995^{+0.061}_{-0.054}$ | $-1.19^{+0.73}_{-0.33}$ | -1.03 ± 0.10 | $-1.04^{+0.21}_{-0.17}$ | -1.021 ± 0.044 |
| | $10^2 \Omega_b h^2$ | 2.235 ± 0.015 | 2.238 ± 0.015 | 2.23 ± 0.49 | 2.235 ± 0.013 | $2.25^{+0.64}_{-0.34}$ | 2.2353 ± 0.0087 |
| CPL | Ω_m | 0.318 ± 0.059 | $0.342^{+0.026}_{-0.029}$ | $0.333^{+0.10}_{-0.076}$ | $0.316^{+0.040}_{-0.054}$ | $0.326^{+0.082}_{-0.056}$ | 0.314 ± 0.023 |
| | h | $0.682^{+0.052}_{-0.076}$ | $0.650^{+0.024}_{-0.027}$ | > 0.653 | 0.680 ± 0.050 | > 0.647 | $0.679^{+0.023}_{-0.026}$ |
| | w_0 | -0.60 ± 0.52 | $-0.68^{+0.27}_{-0.31}$ | -0.78 ± 0.64 | $-0.89^{+0.41}_{-0.53}$ | $-0.77^{+0.37}_{-0.50}$ | -0.98 ± 0.24 |
| | w_a | < -0.592 | $-0.91^{+0.91}_{-0.70}$ | < -0.557 | $-0.49^{+1.4}_{-0.92}$ | $-1.1^{+2.5}_{-1.5}$ | $-0.15^{+0.62}_{-0.54}$ |
| | $10^2 \Omega_b h^2$ | 2.236 ± 0.015 | 2.235 ± 0.015 | $2.54^{+1.0}_{-0.72}$ | 2.236 ± 0.015 | $2.54^{+1.0}_{-0.63}$ | 2.237 ± 0.012 |

NOTE—The errors at the 68.3% confidence level are shown. The fitting results of the cosmological parameters are obtained by using the CMB, CMB+BAO, FRB1, CMB+FRB1, FRB2, and CMB+FRB2 data. Here, *FRB1* and *FRB2* denote the FRB data in the normal expectable scenario (i.e., $N_{\text{FRB}} = 1000$) and the FRB data in the optimistic scenario (i.e., $N_{\text{FRB}} = 10000$), respectively.

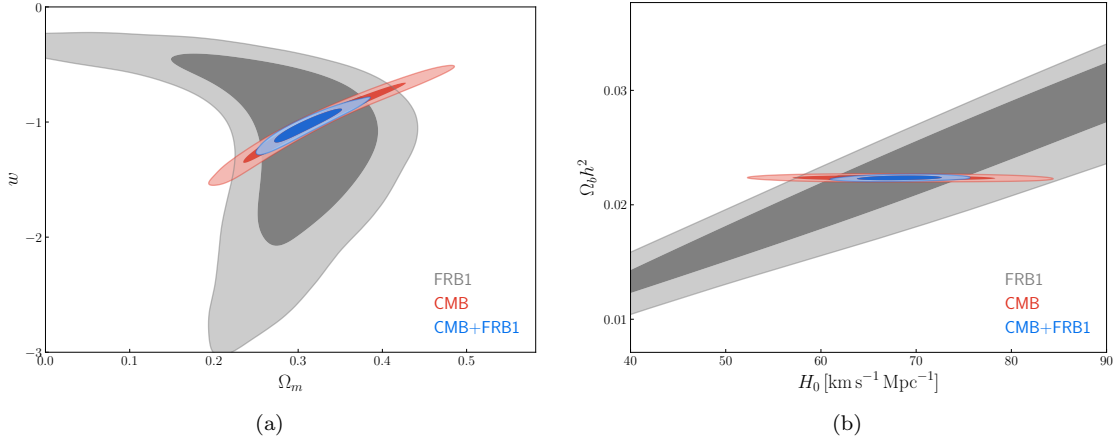


Figure 1. Two-dimensional marginalized contours (68.3% and 95.4% confidence level) in the Ω_m – w plane (left panel) and the H_0 – $\Omega_b h^2$ plane (right panel) for the w CDM model, by using FRB, CMB, and CMB+FRB. Here, for the simulated FRB data, the normal expectable scenario is assumed.

constraints on the parameters compared with those using the GW data alone. For example, compared with the results of the GW data alone, the inclusion of FRB2 data reduces the relative error on Ω_m from 9.0% to 4.2%. We also find that the data combination GW+FRB2 provides the comparable constraints as the CMB+BAO constraints for the parameters Ω_m and $\Omega_b h^2$. For the parameters H_0 and w , we have the constraint errors: $\varepsilon(H_0) = 1.4\%$ and $\varepsilon(w) = 11\%$ from GW+FRB2, and $\varepsilon(H_0) = 2.1\%$ and $\varepsilon(w) = 5.8\%$ from CMB+BAO. Compared with the case of CMB+BAO, the combination of the FRB and GW data provides tighter constraint on H_0

and looser constraint on w . Therefore, the data combination GW+FRB can serve as a low-redshift measure of cosmological parameters, which is fully independent of the CMB and BAO observations.

In fact, the FRB data cannot effectively break the parameter degeneracies formed by the GW data, because H_0 is poorly constrained by using FRB alone when no priors are included. In addition, the standard siren data do not contain the information of Ω_b , thus cannot break the strong degeneracy between H_0 and $\Omega_b h^2$ in FRB. Since the CMB data can measure the baryon density,

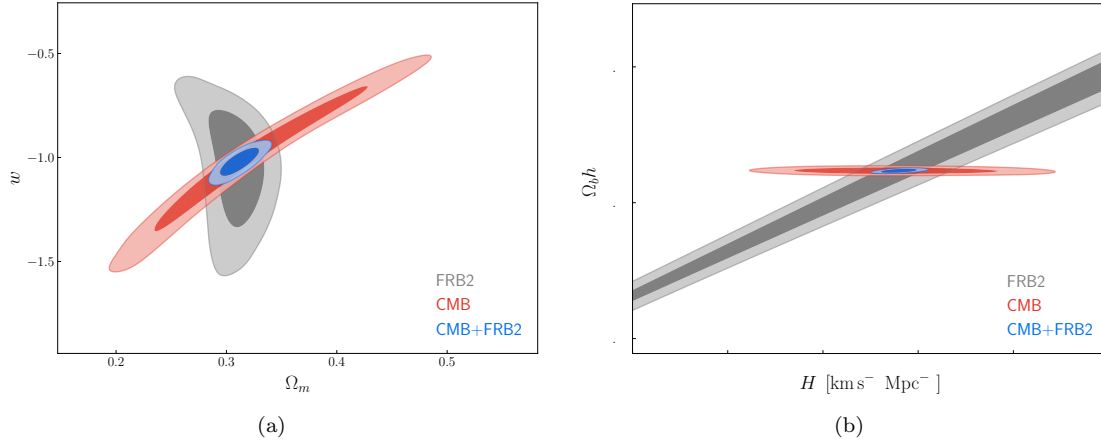


Figure 2. Two-dimensional marginalized contours (68.3% and 95.4% confidence level) in the Ω_m - w plane (left panel) and the H_0 - $\Omega_b h^2$ plane (right panel) for the w CDM model, by using FRB, CMB, and CMB+FRB. Here, for the simulated FRB data, the optimistic scenario is assumed.

Table 2. The 1σ errors on the cosmological parameters in the w CDM model.

| Model | Parameter | GW | GW+FRB | CMB+GW | FRB+CMB+GW |
|-------------|----------------------------|-------|--------|--------|------------|
| w CDM | $\sigma(\Omega_m)$ | 0.028 | 0.024 | 0.0067 | 0.0063 |
| | | | 0.013 | | 0.0057 |
| | $\sigma(h)$ | 0.013 | 0.012 | 0.0075 | 0.0070 |
| | | | 0.0097 | | 0.0062 |
| $\sigma(w)$ | 0.18 | 0.16 | 0.037 | 0.034 | |
| | | | 0.11 | 0.030 | |
| | $10^2\sigma(\Omega_b h^2)$ | ... | 0.022 | 0.014 | 0.012 |
| | | | 0.013 | | 0.0072 |

NOTE—The errors on the cosmological parameters are obtained by using the GW, GW+FRB, CMB+GW, and FRB+CMB+GW data. The two values in a cell in the columns of GW+FRB and FRB+CMB+GW represent the normal expectable scenario and the optimistic scenario of FRB, respectively, from top to bottom.

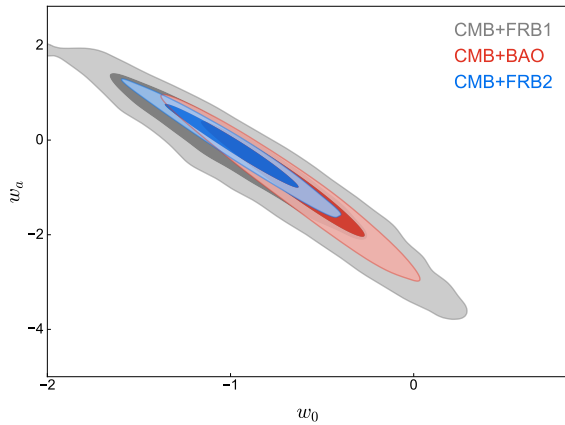


Figure 3. Two-dimensional marginalized contours (68.3% and 95.4% confidence level) in the w_0 - w_a plane for the CPL model, by using CMB+BAO, CMB+FRB1, and CMB+FRB2.

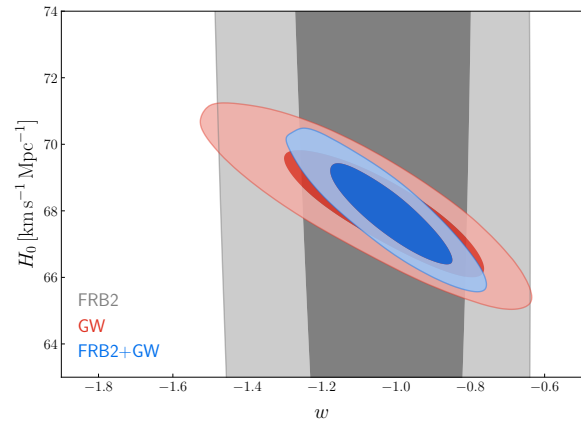


Figure 4. Two-dimensional marginalized contours (68.3% and 95.4% confidence level) in the w - H_0 plane for the w CDM model, by using FRB, GW, and GW+FRB. Here, for the simulated FRB data, the optimistic scenario is assumed.

we further include the CMB data in the combination of FRB+GW as a prior in the next subsection.

3.3. CMB+GW+FRB

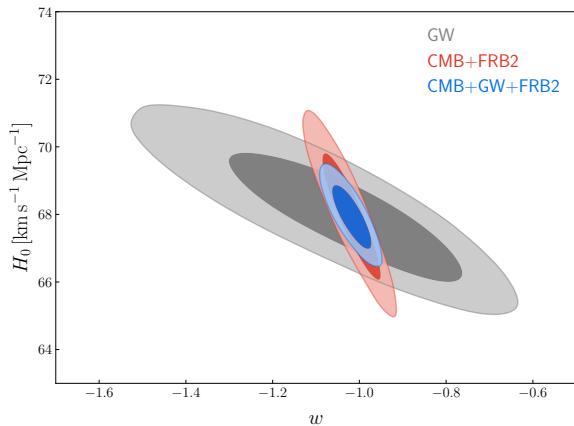


Figure 5. Two-dimensional marginalized contours (68.3% and 95.4% confidence level) in the w - H_0 plane for the w CDM model, by using GW, CMB+FRB, and CMB+GW+FRB. Here, for the simulated FRB data, the optimistic scenario is assumed.

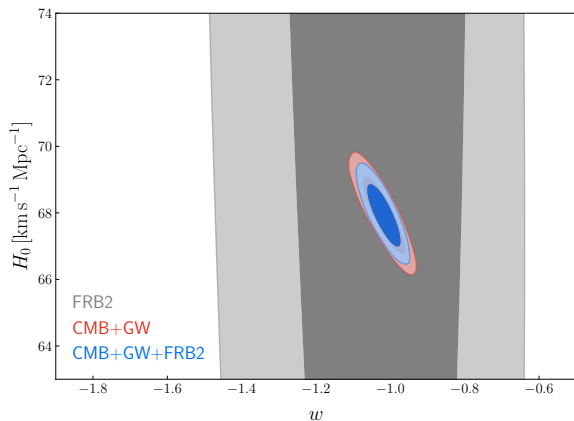


Figure 6. Two-dimensional marginalized contours (68.3% and 95.4% confidence level) in the w - H_0 plane for the w CDM model, by using FRB, CMB+GW, and CMB+GW+FRB. Here, for the simulated FRB data, the optimistic scenario is assumed.

We further investigate the capability of the data combination CMB+GW+FRB on constraining cosmological parameters. The CMB data are used as a prior on $\Omega_b h^2$ to break the strong degeneracy between H_0 and $\Omega_b h^2$ in FRB. We show the constraint contours by using the GW, CMB+FRB2, and CMB+GW+FRB2 data combinations for the w CDM model in Figure 5, which seems to show that the constraints from the combination CMB+GW+FRB are obviously improved than

both GW and CMB+FRB, due to the different orientations of degeneracies.

However, from Figure 6, it is clear that the constraint results from the data combination CMB+GW+FRB are only slightly better than those from CMB+GW. The constraints from the FRB data are too weak compared to those from CMB+GW. This is also indicated by Figure 2(b) in which the parameter degeneracies of the data combination CMB+FRB are determined by CMB, not by FRB. The precise measurement on $\Omega_b h^2$ by CMB leads to DM_{IGM} roughly proportional to $1/H_0$, which is similar to the expression of luminosity distance. Therefore, the effect of FRB to break the parameter degeneracies inherent in GW is not obvious when using CMB as a prior.

Although the combination CMB+GW already provides tight constraints on cosmological parameters, the FRB data can still supplement to them. Since the GW data lack of the information of Ω_b , the most improved constraint by including the FRB2 data is given by $\varepsilon(\Omega_b h^2) = 0.32\%$, which is improved by 49% compared to the result of CMB+GW. Except $\Omega_b h^2$, the constraints on other cosmological parameters are improved only a little even 10000 simulated FRB data are included in the data combination.

4. CONCLUSION

In this work, we study the capability of future FRB data of improving the cosmological parameter estimation. For the event number of FRBs, we consider a normal expectable scenario, i.e., $N_{\text{FRB}} = 1000$, and an optimistic scenario, i.e., $N_{\text{FRB}} = 10000$, as examples. We also consider two dynamical dark energy cosmological models, i.e., the w CDM and CPL models.

We find that, although the FRB data alone cannot effectively constrain H_0 and $\Omega_b h^2$, the combination of the current CMB data and the simulated FRB data can provide rather good constraints on the Hubble constant H_0 and dark energy parameters, due to the fact that FRB is able to break the parameter degeneracies inherent in the CMB data. Both H_0 and the EoS of dark energy w in the w CDM model are improved by about 50% by including the FRB data in the normal expectable scenario, and are improved by about 80% by including the FRB data in the optimistic scenario, compared with those using the CMB data alone. For both the w CDM and CPL models, the optimistic FRB data have better capability, compared with the BAO data, of breaking the parameter degeneracies inherent in the CMB data. Nevertheless, the advantage of the FRB data resides in the better constraint on $\Omega_b h^2$ compared with CMB+BAO.

We also investigate the capability of the combination of the FRB data and the GW standard siren data, another future low-redshift cosmological probe, in cosmological parameter estimation. We find that the constraints on cosmological parameters from the data combination GW+FRB are comparable to those from CMB+BAO. Thus, this combination may provide a novel low-redshift probe of the cosmological parameters, independent of the CMB and BAO data. If we include the current CMB data, the constraints from the combination CMB+GW+FRB seem to be further improved compared to GW and CMB+FRB. However, we find that the dominating contributions to the constraints of the combination CMB+GW+FRB come from CMB+GW. In fact, the bottleneck of the FRB data in cosmology is the strong degeneracy between H_0 and $\Omega_b h^2$. In this case, even though the data combination CMB+GW provides tight constraints, the inclusion of

FRB data can still improve the constraint on $\Omega_b h^2$ evidently. For now, the FRB cosmology is still an open topic, we believe that future plentiful FRB observations will play a significant role in cosmological parameter estimation to supplement and verify the results from other observations.

ACKNOWLEDGMENTS

We are very grateful to Ling-Feng Wang for fruitful discussions. This work was supported by the National Natural Science Foundation of China (Grants Nos. 11975072, 11875102, 11835009, 11690021, 11722324, 11690024, and 11920101003), the Liaoning Revitalization Talents Program (XLYC1905011), the Fundamental Research Funds for the Central Universities (N2005030 and N180503014), and the National Program for Support of Top-Notch Young Professionals (W02070050).

REFERENCES

- Bahcall, N.A., Ostriker, J.P., Perlmutter, S., & Steinhardt, P. J. 1999, *Sci*, 284, 1481
- Bannister, K. W., Deller, A. T., Phillips, C., et al. 2019, arXiv:1906.11476
- Beutler, F., Blake, C., Colless, M., et al. 2011, *MNRAS*, 416, 3017
- BOSS Collaboration, Alam, S., Ata, M., et al. 2017, *MNRAS*, 470, 2617
- Cai, R.G., Liu, T.B., Liu, X.W., Wang, S.J., & Yang, T. 2018, *PhRvD*, 97, 103005
- Cai, R. G., Liu, T. B., Wang, S. J., & Xu, W. T. 2019, *JCAP*, 1909, 016
- Cai, R.G., & Yang T. 2017 *PhRvD*, 95, 044024
- Chatterjee, S., Law, C. J., Wharton, R. S., et al. 2017, *Natur*, 541, 58
- Chen, H.Y., Fishbach, M., & Holz, D.E. 2018, *Natur*, 562, 545
- Chen, L., Huang, Q.-G., & Wang, K. 2019, *JCAP*, 1902, 028
- Chevallier, M., & Polarski, D. 2001, *IJMPD*, 10, 213
- CHIME/FRB Collaboration, Amiri, M., Bandura, K., et al. 2018, *ApJ*, 863, 48
- Cordes, J. M., & Chatterjee, S. 2019, *ARA&A*, 57, 417
- Cutler, C., & Holz, D. E. 2009, *PhRvD*, 80, 104009
- Deng, W., & Zhang, B. 2014, *ApJL*, 783, L35
- Fan, X., Carilli, C. L., & Keating, B. 2006, *ARA&A*, 44, 415
- Faucher-Giguère, C.-A., Kereš, D., & Ma, C.-P. 2011, *MNRAS*, 417, 2982
- Feeney, S.M., Peiris, H.V., Williamson, A.R., et al. 2019, *PhRvL*, 122, 061105
- Fialkov, A., & Loeb, A. 2017, *ApJ*, 846, L27
- Gao, H., Li, Z., & Zhang, B. 2014, *ApJ*, 788, 189
- Holz, D. E., & Hughes, S. A. 2005, *ApJ*, 629, 15
- Jaroszynski, M. 2019, *MNRAS*, 484, 1637
- Jin, S.J., He, D.Z., Xu, Y., Zhang, J.F., & Zhang, X. 2020, *JCAP*, 03, 051
- Joyce, A., Jain, B., Khoury, J., & Trodden, M. 2015, *PhR*, 568, 1
- Kumar P., & Linder, E. V. 2019, *PhRvD*, 100, 083533
- Lewis, A. & Bridle, S. 2002, *PhRvD*, 66, 103511
- Li, H.L., He, D.Z., Zhang, J.F., & Zhang, X. 2019, arXiv:1908.03098, *JCAP* in press
- Li, T.G.F 2015, Springer Theses, <http://link.springer.com/book/10.1007%2F978-3-319-19273-4>
- Li, Z., Gao, H., Ding, X., Wang, G., & Zhang, B. 2018, *NatCo*, 9, 3833
- Li, Z., Gao, H., Wei, J.-J., et al. 2019, *ApJ*, 876, 146
- Linder, E. V. 2003, *PhRvL*, 90, 091301
- Liu, B., Li, Z., Gao H., & Zhu, Z.-H. 2019 *PhRvD*, 99, 123517
- Lorimer, D. R., Bailes, M., McLaughlin, M. A., Narkevic, D. J., & Crawford, F. 2007, *Sci*, 318, 777
- Luo, R., Lee, K., Lorimer, D. R., & Zhang, B. 2018, *MNRAS*, 481, 2320

- Macquart, J. P., Keane, E., Grainge, K., et al. 2015, in Proc. Advancing Astrophysics with the Square Kilometre Array (AASKA14) (Trieste: SISSA), 55
- Manchester, R. N., Hobbs, G. B., Teoh, A., & Hobbs, M. 2005, *AJ*, 129, 1993
- Marcote, B., Paragi, Z., Hessels, J. W. T., et al. 2017, *ApJL*, 834, L8
- McQuinn, M. 2014, *ApJ*, 780, L33
- Petroff, E., Bailes, M., Barr, E. D., et al. 2015, *MNRAS*, 447, 246
- Petroff, E., Barr, E. D., Jameson, A., et al. 2016, *PASA*, 33, e045
- Petroff, E., Hessels, J. W. T., Lorimer, D. R. 2019, *A&ARv*, 27, 4
- Planck Collaboration, Aghanim, N., Akrami, Y., et al. 2018a, arXiv:1807.06209
- Planck Collaboration, Akrami, Y., Arroja, F., et al. 2018b, arXiv:1807.06205
- Ravi, V., Catha, M., D'Addario, L., et al. 2019, arXiv:1907.01542.
- Ross, A. J., Samushia, L., Howlett, C., et al. 2015, *MNRAS*, 449, 835
- Sathyaprakash, B. S., & Schutz, B. F. 2009, *LRR*, 12, 2
- Sathyaprakash, B.S., Schutz, B.F., & Van Den Broeck, C 2010, *CQGra*, 27, 215006
- Schneider, R., Ferrari, V., Matarrese, S., & Portegies Zwart, S. F. 2001, *MNRAS*, 324, 797
- Scholz, P., Spitler, L. G., Hessels, J. W. T., et al. 2016, *ApJ*, 833, 177
- Schutz, B. F. 1986, *Natur*, 323, 310
- Shull, J. M., Smith, B. D., & Danforth, C. W. 2012, *ApJ*, 759, 23
- Spitler, L. G., Scholz, P., Hessels, J. W. T., et al. 2016, *Natur*, 531, 202
- Supernova Search Team, Riess, A. G., Filippenko, A. V., et al. 1998, *AJ*, 116, 1009
- Supernova Cosmology Project, Perlmutter, S., Aldering, G., et al. 1999, *ApJ*, 517, 565
- Tendulkar, S. P., Bassa, C. G., Cordes, J. M., et al. 2017, *ApJL*, 834, L7
- Thornton, D., Stappers, B., Bailes, M., et al. 2013, *Sci*, 341, 53
- Walters, A., Weltman, A., Gaensler, B. M., Ma, Y.-Z., & Witzemann, A. 2018, *ApJ*, 856, 65
- Wang, L.F., Zhang, X.N., Zhang, J.F., & Zhang, X. 2018, *PhLB*, 782, 87
- Wei, J.-J., Wu, X.-F., & Gao, H. 2018, *ApJL*, 860, L7
- Weinberg, S. 1989, *RvMP*, 61, 1
- Yang, Y.-P., & Zhang, B. 2016, *ApJL*, 830, L31
- Yu, H., & Wang, F. Y. 2017, *A&A*, 606, A3
- Yüksel, H., Kistler, M. D., Beacom, J. F., & Hopkins, A. M. 2008, *ApJL*, 683, L5
- Zhang, J.F., Dong, H.Y., Qi, J.Z., & Zhang, X. 2020, *EPJC*, 80, 217
- Zhang, J.F., Zhang, M., Jin, S.J., Qi, J.Z., & Zhang, X. 2019, *JCAP*, 09, 068
- Zhang, X. 2019, *SCPMA*, 62, 110431
- Zhang, X.N., Wang, L.F., Zhang, J.F., & Zhang, X. 2019, *PhRvD*, 99, 063510
- Zhao, W., Van Den Broeck, C, Baskaran, D., & Li T.G.F 2011, *PhRvD*, 83, 023005
- Zhou, B., Li, X., Wang, T., Fan, Y.-Z., & Wei, D.-M. 2014, *PhRvD*, 89, 107303